HAL open science

Aircraft observations since the 1990s reveal increases of tropospheric ozone at multiple locations across the Northern Hemisphere

Audrey Gaudel, Owen Cooper, Kai-Lan Chang, Ilann Bourgeois, Jerry Ziemke, Sarah Strode, Luke D. Oman, Pasquale Sellitto, Philippe Nédélec, Romain Blot, et al.

To cite this version:

Audrey Gaudel, Owen Cooper, Kai-Lan Chang, Ilann Bourgeois, Jerry Ziemke, et al.. Aircraft observations since the 1990s reveal increases of tropospheric ozone at multiple locations across the Northern Hemisphere. Science Advances , 2020, 6 (34), pp.eaba8272. 10.1126/sciadv.aba8272 . hal-02988543

HAL Id: hal-02988543

https://hal.science/hal-02988543

Submitted on 10 Nov 2020

HAL is a multi-disciplinary open access archive for the deposit and dissemination of scientific research documents, whether they are published or not. The documents may come from teaching and research institutions in France or abroad, or from public or private research centers.

L'archive ouverte pluridisciplinaire **HAL**, est destinée au dépôt et à la diffusion de documents scientifiques de niveau recherche, publiés ou non, émanant des établissements d'enseignement et de recherche français ou étrangers, des laboratoires publics ou privés.

CLIMATOLOGY

Aircraft observations since the 1990s reveal increases of tropospheric ozone at multiple locations across the Northern Hemisphere

Audrey Gaudel[1]*, Owen R. Cooper[1], Kai-Lan Chang[1], Ilann Bourgeois[1], Jerry R. Ziemke[2,3], Sarah A. Strode[2,4], Luke D. Oman[2], Pasquale Sellitto[5], Philippe Nédélec[6], Romain Blot[6], Valérie Thouret[6], Claire Granier[1,6]

Copyright © 2020 The Authors, some rights reserved; exclusive licensee American Association for the Advancement of Science. No claim to original U.S. Government Works. Distributed under a Creative Commons Attribution NonCommercial License 4.0 (CC BY-NC).

Tropospheric ozone is an important greenhouse gas, is detrimental to human health and crop and ecosystem productivity, and controls the oxidizing capacity of the troposphere. Because of its high spatial and temporal variability and limited observations, quantifying net tropospheric ozone changes across the Northern Hemisphere on time scales of two decades had not been possible. Here, we show, using newly available observations from an extensive commercial aircraft monitoring network, that tropospheric ozone has increased above 11 regions of the Northern Hemisphere since the mid-1990s, consistent with the OMI/MLS satellite product. The net result of shifting anthropogenic ozone precursor emissions has led to an increase of ozone and its radiative forcing above all 11 study regions of the Northern Hemisphere, despite NO_x emission reductions at midlatitudes.

Downloaded from http://advances.sciencemag.org/ on November 10, 2020

INTRODUCTION

Tropospheric ozone originates from in situ photochemical reactions and transport from the stratosphere (*1*). Because of a lack of ozone observations from preindustrial times, global atmospheric chemistry models must be used to quantify long-term changes of the global tropospheric ozone burden. Ensemble model simulations indicate a global burden increase of 40% since preindustrial times, producing a globally averaged radiative forcing (RF) of 0.40 ± 0.20 W m^{-2} and making tropospheric ozone the third most effective anthropogenic climate forcer after CO_2 and CH_4 (*2*). The relatively large uncertainty of this estimate (±50%) is mainly due to the lack of observations to constrain the model estimates of preindustrial ozone. However, a recent proxy-based study relying on the isotopic composition of oxygen in ice cores corroborates these model results (*3*). New analysis by the Tropospheric Ozone Assessment Report (TOAR) (*4*) assessed the historical ozone records from the early and mid-20th century and concluded that surface ozone at midlatitudes and high latitudes of the Northern Hemisphere increased by 30 to 70%, with large uncertainty, between the historical period and the modern period (1990–2014); limited historical observations indicate similar increases in the free troposphere (FT) of northern midlatitudes. Intergovernmental Panel on Climate Change [IPCC; AR5, section 2.2.2.3] assessed the available evidence for tropospheric ozone trends through the year 2010 and concluded that ozone across the Northern Hemisphere had generally increased since the 1970s at the surface and in the FT (*2*). With regard to trends since the 1990s, TOAR showed that observations have been insufficient for the detection of an unambiguous trend in the global tropospheric ozone burden over the past two decades (*5*); in particular, the available satellite products have disagreed on the sign of the trend since 2008. TOAR took advantage of the IAGOS (In-Service Aircraft for a Global Observing System) database (*6*), which contains ozone observations from more than 60,000 commercial aircraft flights worldwide, to quantify ozone trends above five regions of the Northern Hemisphere (northeastern United States, Germany, India, Southeast Asia, and Northeast China/Korea) during 1994–2014. Relatively weak ozone increases (<7% $decade^{-1}$) occurred above northeastern United States and Germany but not at all tropospheric levels and not in all seasons. However, ozone increased in all seasons and at most levels above the three Asian regions (4 to 70% $decade^{-1}$). An independent analysis of IAGOS observations reported widespread upper tropospheric ozone increases above several regions in the northern midlatitudes for the period 1994–2013 (4 to 5% $decade^{-1}$), but the study did not address the tropics or the lower or mid-troposphere (MT) (*7*). Global chemistry climate models indicate that the tropospheric ozone burden and its associated RF have continued to increase since 1990 (*2*, *8*). However, confirmation of these recent global-scale increases from in situ observations has been difficult because of limited monitoring in the FT and at remote surface locations, compounded by the various and contradictory trend results described above. To improve our understanding of ozone trends across the Northern Hemisphere, this new study expands the TOAR analysis by including two additional years of IAGOS data (2015–2016) and six new regions (western North America, South America, Gulf of Guinea, the Persian Gulf, and Malaysia/Indonesia) (Fig. 1), using 2.5 times as much IAGOS data as the earlier TOAR study. By expanding the analysis to a wider spatial coverage and spanning up to 22 (1994–2016) years of observations made from consistent and routinely calibrated instruments (ultraviolet absorption method), we can now show that ozone has increased at 11 of 11 study regions widely distributed across the Northern Hemisphere, advancing our understanding of Northern Hemisphere ozone changes beyond the more limited TOAR analysis.

[1]CIRES, University of Colorado/NOAA Chemical Sciences Laboratory, Boulder, CO, USA. [2]NASA Goddard Space Flight Center, Greenbelt, MD, USA. [3]Morgan State University, Baltimore, MD, USA. [4]Universities Space Research Association, Columbia, MD, USA. [5]Laboratoire Interuniversitaire des Systèmes Atmosphériques, UMR CNRS 7583, Université Paris-Est Créteil, Université de Paris, Institut Pierre Simon Laplace, Créteil, France. [6]Laboratoire d'Aérologie, Université de Toulouse, CNRS, UPS, France.
*Corresponding author. Email: audrey.gaudel@noaa.gov

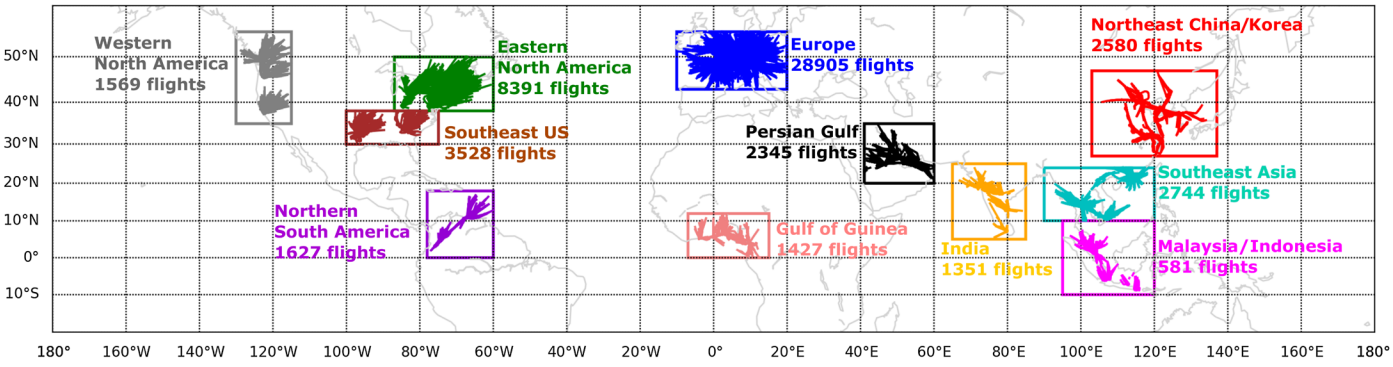

Fig. 1. Map of the 11 study regions. The flight tracks are also indicated in the boxes with western North America in gray, eastern North America in green, Europe in blue, Northeast China/Korea in red, southeast United States in brown, northern South America in purple, Gulf of Guinea in salmon, the Persian Gulf in black, India in orange, Southeast Asia in cyan, and Malaysia/Indonesia in magenta.

MATERIALS AND METHOD

IAGOS data

The IAGOS program is a European Research Infrastructure that has measured ozone worldwide since 1994, using instruments onboard commercial aircraft of internationally operating airlines (*6*). Ozone is measured on all flights using a dual-beam ultraviolet absorption monitor (time resolution of 4 s) with an accuracy estimated at about ±(2 nmol mol^{-1} + 2%) (*9*, *10*). Because most IAGOS aircraft have belonged to airlines based in Europe since the program's inception, Western Europe is the program's most frequently sampled region of the world. Above northwestern Europe (0°E to 15°E, 47°N to 55°N) IAGOS aircraft measured 34,600 ozone profiles between 1994 and 2016, which are approximately four profiles per day. IAGOS aircraft takeoff and land at any time of day and data from all hours of the day are used in this analysis. An analysis of the high-frequency European ozone profiles shows that there is no diurnal ozone cycle in the FT (above the 750-hPa level), although a clear ozone cycle occurs in the boundary layer, and is strongest below 950 hPa (*11*). To avoid the impact of the strong diurnal ozone cycle at the surface, all ozone observations below the 950-hPa level were removed from the analysis. In addition, any observations within 300 m of the surface were also removed. To avoid the influence from the lower stratosphere, all observations in the stratosphere or the tropopause layer (*7*) were removed from the analysis. The tropopause was defined with respect to potential vorticity and was determined by the pressure of the 2-PVU (potential vorticity units) surface. The lower bound of the tropopause layer was then defined as the pressure of the 2-PVU surface + 15 hPa. Any ozone observation with a pressure value less than the lower bound of the tropopause layer was removed from the dataset. The 11 study regions (Fig. 1) were chosen because they were the only regions available with frequent sampling in both the early (1994–2004) and late periods (2011–2016) between 1994 and 2016, which allows the calculation of ozone changes over periods spanning two decades (see table S1). For the years 2005–2010, several regions have large data gaps, and therefore, we did not include these years when comparing all regions. However, the ozone trend values (see the "Trend calculation" section) are based on all available ozone profiles, and they are not dependent on the choice of the early and late periods. The length of these time series (>20 years) is advantageous because they are long enough to largely overcome the influence of internal climate variability, such as El Niño–Southern Oscillation (*12*), on long-term ozone trends (*13*). However, we cannot rule out some impact from internal climate variability on the observed trends.

Several studies over the past 20 years have examined the regional representativeness of IAGOS observations (*4*, *9*, *14*–*17*) and have established that the data compare well to regional surface and free tropospheric ozonesonde records and that the data are not biased. For example, a recent study showed that IAGOS observations above Europe are representative of regional-scale surface ozone observation across Western Europe (*15*). They evaluated IAGOS ozone observations against rural ozone monitoring sites at low and high elevations across a broad region of Western Europe. They concluded that the IAGOS data are not biased:

> "Based on 11 years of data (2002–2012), this study thus demonstrates that IAGOS observations in the lowest troposphere can be used as a complement to surface stations to study the air quality in/around the agglomeration, providing important information on the vertical distribution of pollution."

The strong winds and the high meteorological variability in the MT and upper troposphere (UT), coupled with ozone's long lifetime [several weeks in the FT (*1*)] relative to transport time scales, also make IAGOS observations representative of the FT. There is no obvious influence from aircraft pollution in the flight corridors that span broad regions of the Northern Hemisphere and are also routinely sampled by ozonesondes and satellites. Previous studies have demonstrated that IAGOS ozone observations in the upper troposphere–lower stratosphere (UTLS) are consistent with ozonesonde observations (*4*, *16*, *17*). The internal consistency of IAGOS observations (between IAGOS aircraft following each other) has been continually monitored and ensured by the IAGOS engineers. Changes of the flight routes with time, especially between 1994–2004 and 2011–2016, can occur because of changes in airports. However, these changes do not affect the average ozone variability in each region as the regions are always fully sampled with time.

MERRA-2 GMI global atmospheric chemistry model

The atmospheric chemistry model simulation in support of this analysis is the Modern-Era Retrospective analysis for Research and Applications version 2 (MERRA-2) Global Modeling Initiative (GMI) simulation (https://acd-ext.gsfc.nasa.gov/Projects/GEOSCCM/MERRA2GMI/), produced with the Goddard Earth Observing System

Downloaded from http://advances.sciencemag.org/ on November 10, 2020

(GEOS) modeling framework (*18*). The MERRA-2 GMI simulation is a dynamically constrained replay (*19*) using winds, temperature, and pressure from the MERRA-2 reanalysis (*20*). Interactive chemistry is included via the GMI's stratospheric and tropospheric chemical mechanism (*12*, *21*, *22*). The GMI mechanism includes a detailed description of ozone-NO_x-hydrocarbon chemistry and has more than 100 species and approximately 400 chemical reactions. The MERRA-2 GMI simulation was run from 1980 to 2016 at ~50-km horizontal resolution (c180) on the cubed sphere and output at the MERRA-2 resolution of 0.625° longitude × 0.5° latitude. It was previously used to interpret long-term positive trends of tropospheric column ozone (TCO) across the tropics, as detected by Total Ozone Mapping Spectrometer/Ozone Monitoring Instrument (OMI)/Microwave Limb Sounder (MLS)/Ozone Mapping and Profiler Suite satellite retrievals over the period 1979–2016 (*23*). Further details of the model, including global emission inventories, are provided in the publication describing the original simulation (*23*).

To understand the drivers of the observed ozone changes, we analyzed the emission inventories of NO_x, used as input for the MERRA-2 GMI model simulation (see Discussion, "Changes in the sources of ozone"). The fossil fuel and biofuel NO_x emissions follow the methodology of the Chemistry-Climate Model Initiative (CCMI): MACCity (*24*) until 2010 and RCP8.5 (representative concentration pathway for a possible range of radiative forcing of 8.5 W m^{-2} in the year 2100) after 2010. Recent decreases in anthropogenic NO_x emissions in China after 2012 (*25*, *26*), as revealed by satellite observations, are not well represented. We also analyzed biomass burning NO_x emissions from the Global Fire Emissions Data version 4s (*27*) and lightning NO_x emissions based on the scheme of Allen *et al.* (*28*), as used by the MERRA-2 GMI simulation. NO_x emissions from international shipping were not used by the model because of difficulties in simulating ozone photochemistry in narrow ship plumes by a relatively coarse global-scale model (*29*). This omission leads to an underestimate of ozone production in the marine boundary layer in regions with heavy ship traffic, such as the South China Sea. We converted all NO_x emissions to units of kg NO km^{-2} $year^{-1}$ or Tg NO $year^{-1}$ (e.g., fig. S9).

To analyze the impact of stratospheric influence on the tropospheric ozone in the model, we used a stratospheric ozone tracer (*30*), which is calculated online in the MERRA-2 GMI model. The tracer is set to the regular ozone values above the tropopause and may be advected into the troposphere via the model circulation. Once the tracer enters the troposphere, it undergoes chemical loss based on the reaction rates for the major ozone loss processes and dry deposition at the surface. For each grid cell, both the World Meteorological Organization lapse rate (temperature lapse rate < 2 K km^{-1}) and the potential vorticity threshold [first occurrence of potential vorticity < 3 PVU from above] are used to assess the tropopause level. The tropopause is determined from the maximum pressure (or lowest altitude) between the two methods. In general, the temperature lapse rate method dominates in the tropics, while the potential vorticity threshold dominates in the extratropics.

Trend calculation

For each IAGOS region and for 15 pressure surfaces spaced every 50 hPa from 950 to 200 hPa, we first calculated monthly mean ozone values and used these monthly means to construct a mean 1994–2016 seasonal cycle. This mean seasonal cycle was then used to deseasonalize the individual IAGOS observations on the same pressure level. The linear trend was then calculated using all available ozone profiles between September 1994 and December 2016 (1998–2016 for the Persian Gulf) using the quantile regression method (*31*). The deseasonalization step reduces the impact of autocorrelation; the remaining autocorrelation can be accounted for in the quantile regression method, but it requires an aggregation of profiles into the monthly time scale (e.g., the autocorrelation structure cannot be imposed on data with multiple measurements on the same time scale). However, this aggregation would substantially reduce the sample size and prevents us from accurately estimating extreme quantiles; therefore, this additional step to further reduce autocorrelation was not taken. Quantile regression is known for its tolerance to a greater number of outliers because it is based on rank values of the sample distribution rather than mean values, and it is considered to be a robust approach when the record may contain many intermittent missing values (*32*–*34*). As the temporal distribution of IAGOS profiles in a given region can be highly intermittent, the quantile regression method is well suited for this dataset.

Each trend is reported as the linear ozone rate of change over the period 1994–2016 in units of nmol mol^{-1} $decade^{-1}$. Each trend value is accompanied by its P value (table S1), which is the probability under a specified statistical model that a statistical summary of the data would be equal to or more extreme than its observed value (*35*). Following the recent recommendation of the American Statistical Association (*36*) and as recently discussed in the journal *Nature (37)*, we report all P values and do not use thresholds, such as $P < 0.05$, to determine whether a trend is statistically meaningful.

OMI/MLS tropospheric column ozone product

This study also examines long-term (2004–2019) TCO trends derived from the OMI and MLS onboard the NASA Aura polar-orbiting satellite (*23*). Calculation of TCO requires subtraction of MLS stratospheric column ozone from OMI total ozone for near–clear sky scenes (OMI radiative cloud fractions less than 30%), yielding a 1.0° latitude × 1.25° longitude gridded product. The OMI/MLS ozone product is available at monthly temporal resolution and can be downloaded from the NASA Goddard Space Flight Center: https://acd-ext.gsfc.nasa.gov/Data_services/cloud_slice/.

RESULTS

Tropospheric ozone increases above 11 polluted regions

During the past 22 years, median ozone values have increased in the FT (700 to 300 hPa) above all 11 study regions (Fig. 2 and table S1) by 2 nmol mol^{-1} $decade^{-1}$ (5% $decade^{-1}$) on average and varying between 1.2 nmol mol^{-1} $decade^{-1}$ (2.4% $decade^{-1}$) above Gulf of Guinea and 5.6 nmol mol^{-1} $decade^{-1}$ (13.5% $decade^{-1}$) above Southeast Asia. Similar results are obtained when considering the full TCO (950 to 250 hPa) (Fig. 2 and table S1). The largest TCO increases occurred above Malaysia/Indonesia (18.5% $decade^{-1}$), Southeast Asia (13.5% $decade^{-1}$), and India (11% $decade^{-1}$), followed by Northeast China/Korea (5.8% $decade^{-1}$) and the Persian Gulf (5.7% $decade^{-1}$) (table S1). With the exception of Northeast China/Korea, TCO increases above the midlatitude regions (North America and Europe) are much less (<3.4% $decade^{-1}$). FT ozone trends are broken down by the cold season (October to March) and the warm season (April to September), with Northeast China/Korea, the Persian Gulf, and Southeast Asia having much larger trends during the warm season (fig. S1).

Downloaded from http://advances.sciencemag.org/ on November 10, 2020

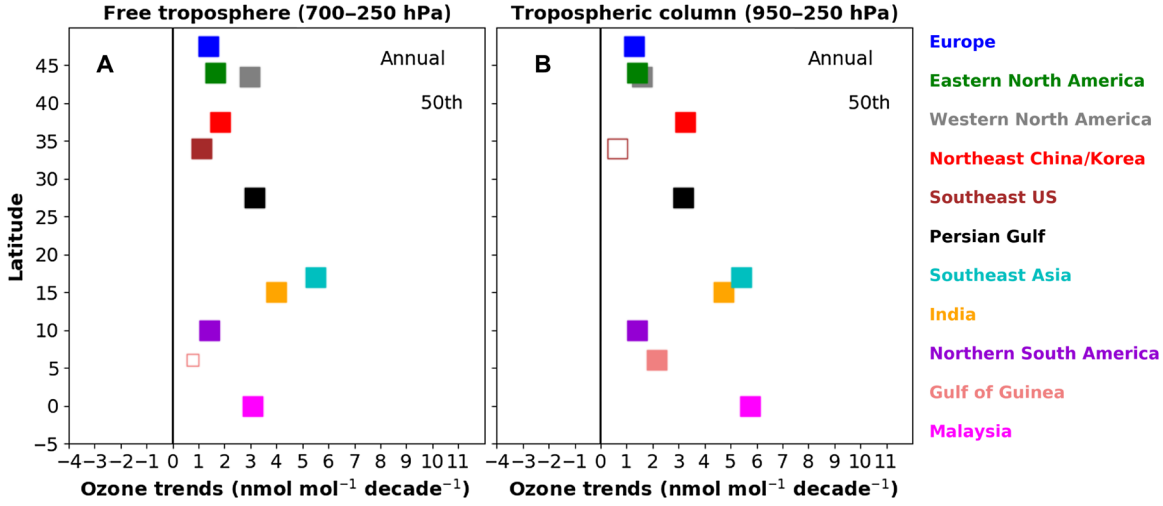

Fig. 2. Annual trends of median ozone (nmol mol^{-1} decade^{-1}) for two columns definition in the troposphere. Trends in the free troposphere (700 to 250 hPa) are shown in (**A**) and trends in the tropospheric column (950 to 250 hPa) are shown in (**B**). The trends are calculated between 1994 and 2016 above western North America (gray), eastern North America (green), Europe (blue), Northeast China/Korea (red), southeast United States (brown), South America (purple), Gulf of Guinea (salmon), India (orange), and Southeast Asia (cyan); between 1998 and 2016 above the Persian Gulf (black); and between 1995 and 2016 above Malaysia/Indonesia (magenta). For South America, the lower limit of the columns is at 600 hPa for data availability. Large squares indicate trends with *P* values less than 0.05; open large squares indicate trends with *P* values between 0.05 and 0.1, and open small squares indicate *P* values greater than 0.1.

These results are consistent with OMI/MLS satellite measurements of TCO (table S1) for the time periods 2004–2016 and 2004–2019, which show widespread increases of ozone across much of the Northern Hemisphere (*23*). Because of the different time periods (the OMI/MLS record only begins in 2004), the IAGOS and OMI/MLS trends are not directly comparable. However, when the OMI/MLS data are extracted above the 11 study regions, they show stronger trends above the tropical regions and Northeast China/Korea compared to the North American and European regions, in general agreement with the IAGOS trends.

Tropospheric ozone changes in the lower troposphere

In this study, the lower troposphere (LT) is defined as the pressure level range of 950 to 800 hPa, which includes most of the boundary layer. In comparison to the FT, the LT presents a wide range of extreme ozone values. The greatest 95th percentiles in recent years (2011–2016) have occurred in the LT above Northeast China/Korea, exceeding 100 nmol mol^{-1}, and also above Southeast Asia, Malaysia/Indonesia, the Persian Gulf, and Gulf of Guinea (Fig. 3D). In all of these regions, except Gulf of Guinea, the warm season values are even greater, reaching 110 nmol mol^{-1} above Northeast China/Korea (fig. S3). The lowest values in recent years (2011–2016) are found in the LT above the tropical regions of India, Southeast Asia, Gulf of Guinea, and Malaysia/Indonesia, where the first percentile is typically below 20 nmol mol^{-1} (see discussion in the "Impacts on radiative forcing" section).

Figure 3A provides vertical information on the annual trends, showing much larger positive trends in the LT than in the FT above India, Malaysia/Indonesia, Northeast China/Korea, Gulf of Guinea, and the Persian Gulf, ranging from 4.9 to 8.3 nmol mol^{-1} decade^{-1} (9.6 to 26.3% decade^{-1}) (table S4). Despite reductions of ozone precursor emissions (*38*), median LT ozone above Europe increased (2.9% decade^{-1}) at a rate similar to the FT rate, while median LT ozone above the three North American regions is largely unchanged over the 1994–2016 period. Several recent studies have shown that reductions of ozone precursors in North America have been most effective at reducing surface ozone levels at the high end of the ozone distribution (*5*, *39*, *40*), especially during the warm season. Accordingly, the annual 95th percentile has decreased in the LT above the three North American regions (Fig. 3B), and these decreases are even greater when focusing on the warm season in both North America and Europe (fig. S2). Overall, the LT trends above North America, Europe, and East Asia from IAGOS measurements are similar to regional trends based on surface observations (*40*). While precursor reductions have been effective at reducing the high ozone events at the surface and in the LT, TCO trends above North America and Europe are largely positive, driven by the free tropospheric ozone increases (Fig. 2). In terms of relative increases, median LT ozone has increased by 30% or more above Northeast China/Korea, Southeast Asia, Gulf of Guinea, India, and Malaysia/Indonesia, with mid-tropospheric increases of 30 to 40% above Southeast Asia and Malaysia/Indonesia for the entire time period (fig. S2).

The MERRA-2 GMI simulation yields ozone trends for the same time period 1994–2016 with similar seasonal and spatial patterns as the observations, e.g., larger positive trends in the FT during the warm season and warm season decreases in the LT above eastern North America and Europe (figs. S4 and S5). Overall, modeled ozone trends most closely resemble the observed trends in the FT of mid-latitudes. However, we also found some important differences between the observed and modeled ozone trends. As shown in fig. S6, the modeled ozone trends are generally less than the observed trends. The greatest model biases are above the tropical regions of India, Southeast Asia, and Malaysia/Indonesia, where the modeled trends are 3 to 5 nmol mol^{-1} decade^{-1} less than the observed trends, based on annual data. The discrepancy is even greater in the LT where the model sees little of the strong observed trends in the tropics or in Northeast China/Korea. The most likely explanation for the low bias in the tropics is an underestimation of ozone precursor emissions trends. Further discussion of the differences between the observed and modeled ozone trends is provided in the next section.

Downloaded from http://advances.sciencemag.org/ on November 10, 2020

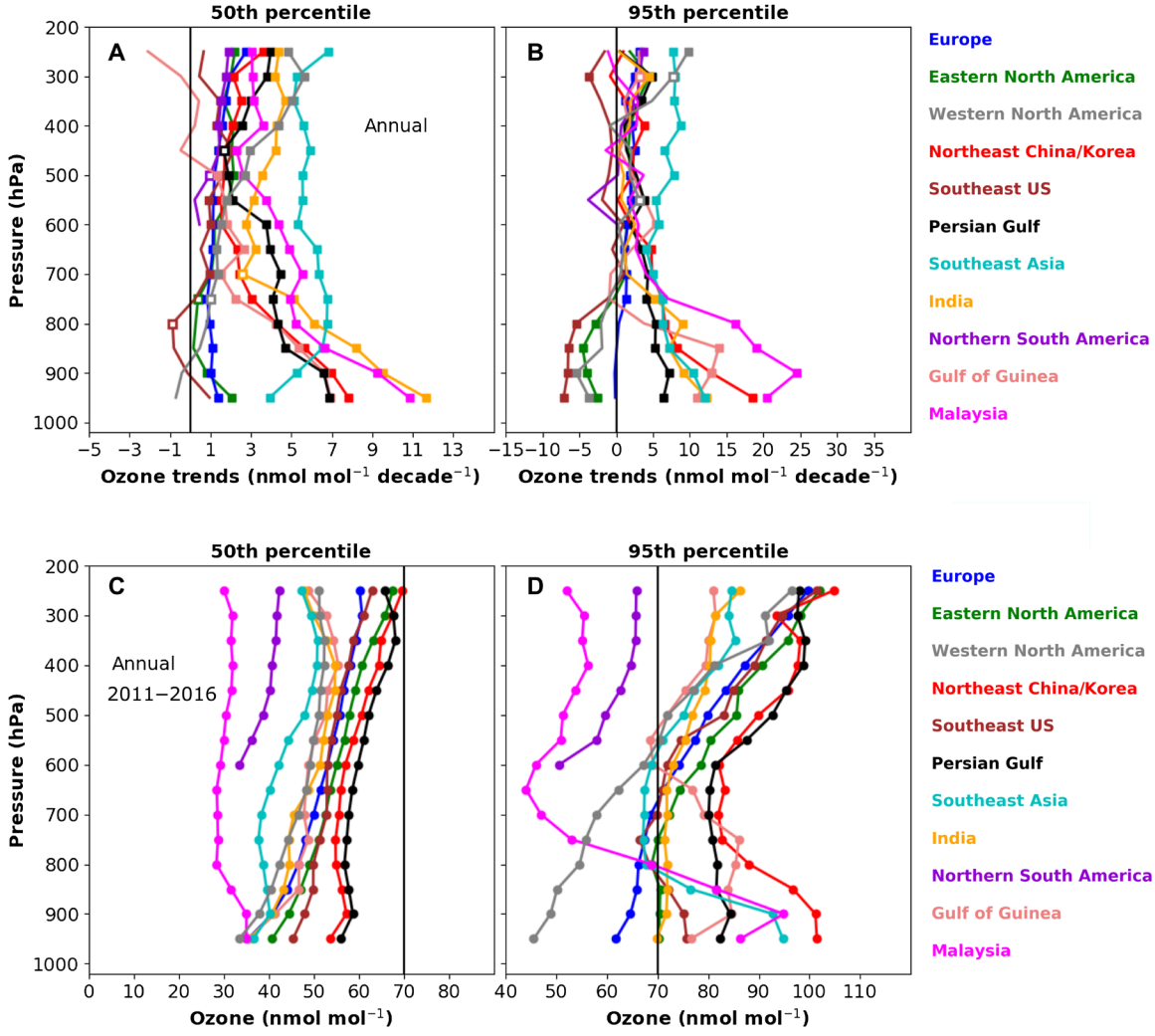

Fig. 3. Annual trends and distribution of the 50th and 95th percentiles of ozone (nmol mol^{-1} decade^{-1}) at intervals of 50 hPa. The trends (**A** and **B**) are calculated between 1994 and 2016 above western North America (gray), eastern North America (green), Europe (blue), Northeast China/Korea (red), southeast United States (brown), South America (purple), Gulf of Guinea (salmon), India (orange), and Southeast Asia (cyan); between 1998 and 2016 above the Persian Gulf (black); and between 1995 and 2016 above Malaysia/Indonesia (magenta). Squares indicate trends with *P* values less than 0.05. Open squares indicate trends with *P* values between 0.05 and 0.1. The zero trend value is indicated with a vertical black bar. The annual profiles of absolute values of ozone (**C** and **D**) are for the recent period 2011–2016 above the same 11 regions. For reference, the 70 nmol mol^{-1} value is indicated with a vertical black line, which corresponds to the U.S. National Ambient Air Quality Standards for ozone and is the annual fourth-highest daily maximum 8-hour average concentration averaged over 3 years.

Notable increases of the lowest ozone values

In addition to the near-consistent positive trends of the median ozone values above all regions, the lowest ozone values (first and fifth percentiles) have also increased above all regions and at most levels (Fig. 4 and fig. S7). The largest increases, throughout the depth of the troposphere, have occurred above India, Southeast Asia, and Malaysia/Indonesia, mostly in the range of 4 to 8 nmol mol^{-1} decade^{-1}. In the early part of the record (1994–2004), ozone values less than 10 nmol mol^{-1} were common in the LT and MT of these regions, but today, these low values have largely disappeared. For example, values less than 20 nmol mol^{-1} in the FT above Malaysia/Indonesia diminished from 24% of all observations during 1994–2004 to just 6% during 2011–2016 (fig. S8A). We found that this phenomenon has also occurred above the remote tropical Pacific Ocean, where the frequency of low ozone observations decreased from 25 to 15% over 20 years, based on airborne research missions (fig. S8B). Such increases have also been recorded by ozonesondes in the FT above Hilo, Hawaï (fig. S7). Observations from the 1970s through the 1990s established that the marine boundary layer of the North Pacific, South Pacific, and Indian Oceans was a broad region of low ozone values, especially in the tropics (*41–44*). Ozone values below 10 nmol mol^{-1} were commonly observed in the tropics because of net chemical destruction in an environment with limited ozone precursors. Tropical deep convection routinely transports ozone-depleted air from the marine boundary layer to the MT and UT (*45–47*), where it can then be transported to midlatitudes (*48–50*). For example, a transport climatology for marine boundary layer observations at the midlatitude site of Bermuda in the North Atlantic Ocean demonstrated that the lowest ozone observations originate at low latitudes (*51*) and the lowest ozone values in the UT above the Eastern United States originate at low latitudes (*52*). Furthermore, an analysis using 3.9 billion back trajectories to explore the transport

Downloaded from http://advances.sciencemag.org/ on November 10, 2020

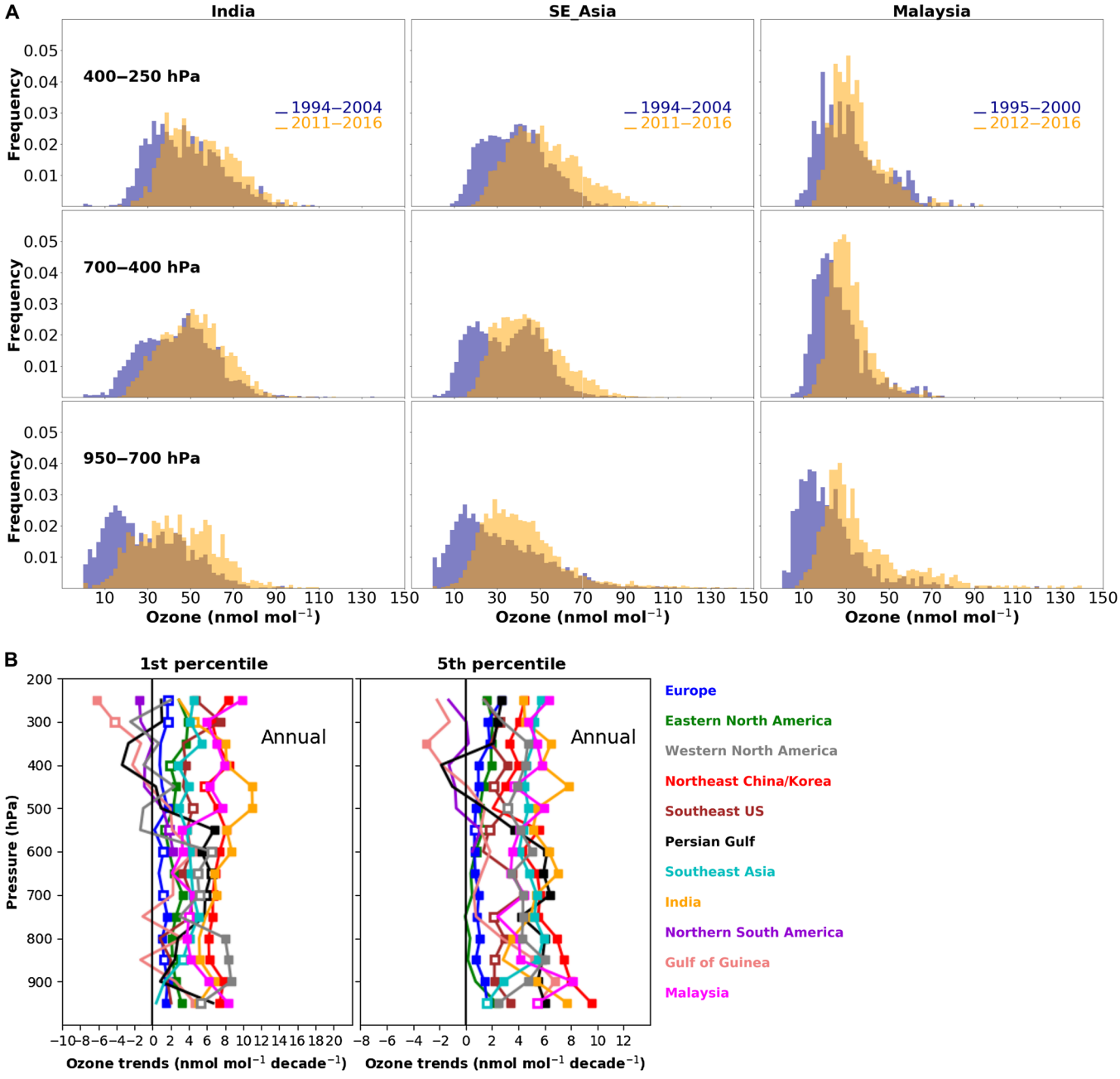

Fig. 4. Histograms of ozone at three levels in the troposphere and for three key tropical regions, India, Southeast Asia, and Malaysia. (**A**) The periods 1994–2004 (blue) and 2011–2016 (orange) are shown above all three sites, with the exception that the earlier period is limited to 1995–2000 above Malaysia/Indonesia because of data availability. (**B**) Also shown are the annual trends of the first and fifth percentiles above all 11 regions, at vertical intervals of 50 hPa. Squares indicate trends with *P* values less than 0.05. Open squares indicate trends with *P* values between 0.05 and 0.1.

pathways associated with ozone observations in the FT above western North America (more than half of the observations were provided by IAGOS) showed that the lowest ozone values are typically associated with a low-latitude origin above the North Pacific Ocean (*53*). That analysis was based on all available springtime ozone observations above western North America, which showed a positive trend from 1984 to 2008.

The western Pacific warm pool, located in the tropics and centered between the International Date Line and Indonesia, has the highest sea surface temperatures in the open oceans (*17*). Intense deep convection above the warm pool produces very low tropospheric column and upper tropospheric ozone values, which on average, are the lowest on Earth (*5*, *46*, *54*–*56*). The clear increases of the lowest ozone values above the warm pool and above the other tropical and midlatitude study regions indicate that there may have been a broad shift in the ozone budget of the Northern Hemisphere since the mid-1990s, especially in regions where ozone destruction once dominated.

Downloaded from http://advances.sciencemag.org/ on November 10, 2020

DISCUSSION

Changes in the sources of ozone

A recent analysis using the Community Atmosphere Model with Chemistry (Cam-chem) global atmospheric chemistry model determined that the shift in ozone precursor emissions from midlatitudes toward the equator produced an increase in the Northern Hemisphere ozone burden from 1980 to 2010, with greater increases above the tropics and East Asia and weaker increases above North America and Europe (*57*). The broad increase of ozone was due to greater ozone production efficiency at low latitudes compared to midlatitudes. To understand whether this same phenomenon applies to our later study period of 1994–2016, we analyzed the emission inventories used by the NASA MERRA-2 GMI model (Fig. 5 and fig. S9). NO_x emission inventories from fossil fuel and biofuel show a clear equatorward shift similar to what was found in the previous study (*57*) and can explain the ozone increases in the LT above the tropical regions (Fig. 3A and fig. S4). While NO_x emissions from biomass burning have decreased in the tropics, the decrease was overcompensated by the increase of fossil fuel emissions (Fig. 5).

Changes in NO_x emissions from lightning are an order of magnitude less than changes of NO_x emissions from fossil fuel combustion, with some regions showing small increases and others showing small decreases (fig. S9D). These model estimated changes in lightning NO_x emissions over the 22-year study period are within the range of other model estimates (*58*). Given the small and variable magnitude of the changes in lightning NO_x emissions, they are not expected to play a major role in the observed ozone trends.

The emission inventory used in the MERRA-2 GMI model does not take into account the recent decreases of precursors of ozone above China, as revealed by satellite observations of tropospheric column NO_2. To explore the impact of reduced emissions from China, we conducted a sensitivity test in which we reduced anthropogenic NO_x emissions by 23% above China for the year 2015, in proportion to the observed decreases from 2012 to 2015 reported by van der A *et al.* (*59*). This adjustment diminished the overall 1994–2016 increase of ozone by 2 to 3 nmol mol^{-1} throughout the troposphere above China and extending into the North Pacific Ocean. However, the response of tropospheric ozone to NO_x reductions in China is complex. For example, during the cold season (October to April) in Northeast China, reduction of anthropogenic NO_x emissions actually led to increases of ozone across the region in the LT, as there was less ozone titration by NO_x during the darker and cloudier conditions of winter. Furthermore, observational evidence from the extensive Chinese surface ozone monitoring network shows that ozone increased across 74 urban areas from 2013 to 2017 (*60*). Another recent study, using the GEOS-Chem model, showed

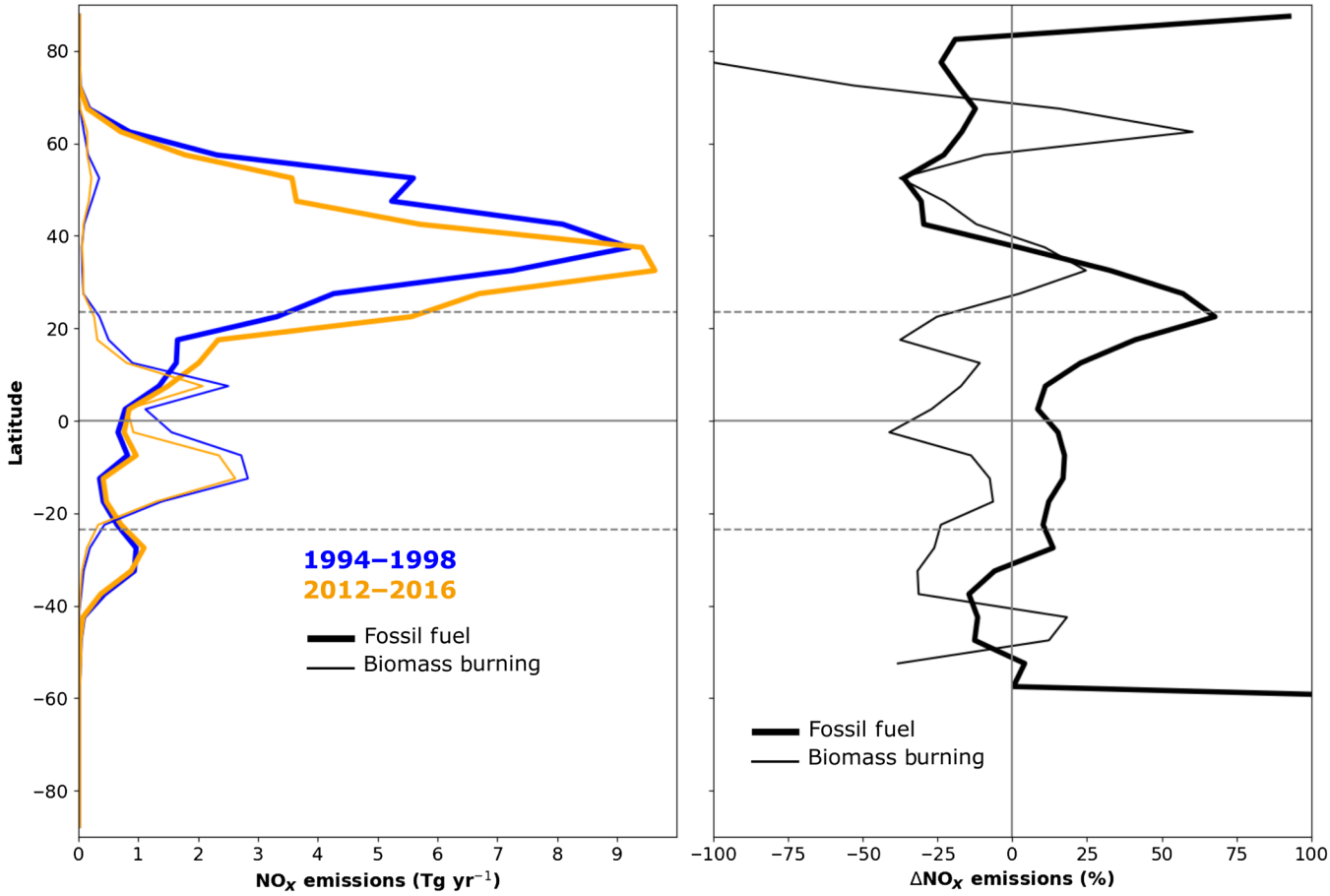

Fig. 5. Latitudinal distribution of NO_x emissions from fossil fuel and biomass burning along with the emissions differences between 1994–1998 and 2012–2016. The emissions are shown in Tg NO $year^{-1}$ for 1994–1998 in blue and 2012–2016 in orange (left). The emissions differences between the two time periods are shown in % (right). For both panels, the latitude band resolution is 5°.

Downloaded from http://advances.sciencemag.org/ on November 10, 2020

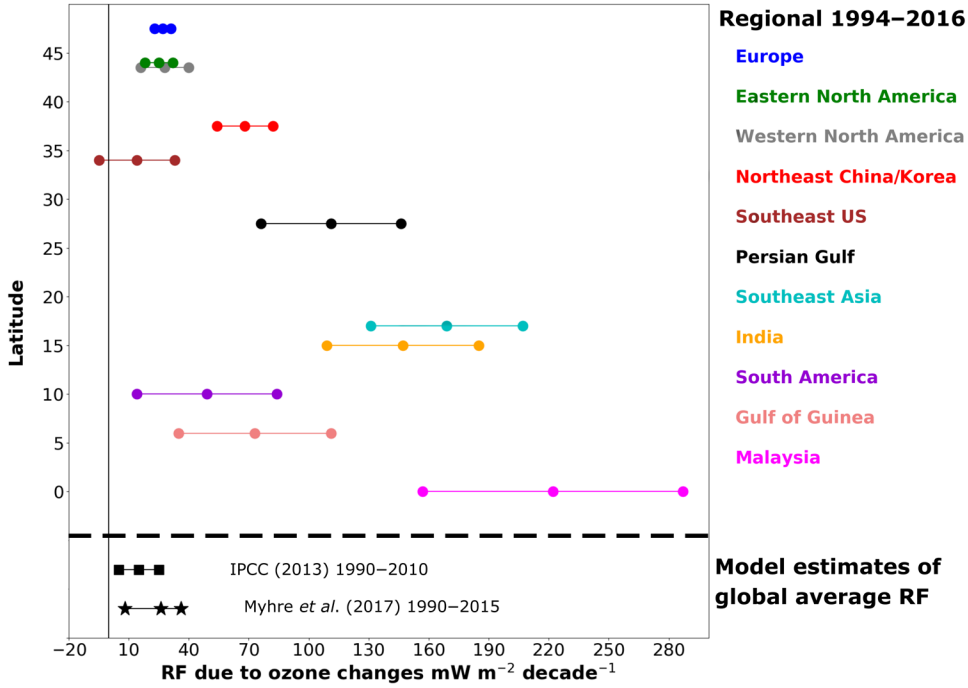

Fig. 6. RF due to ozone above the 11 regions and globally. The circles and bars show the average RF and its range of uncertainty for the 11 regions. The squares and bars show the global average RF and its range of uncertainty from IPCC (2013) (*2*), and the stars and bars show the global average RF and its range of uncertainty from the work of Myhre *et al.* (*8*).

that ozone in megacities of the North China Plain is still increasing despite reductions of ozone precursor emissions (*61*). This contradictory effect was attributed to PM2.5 decreases of 30 to 40% from 2013 to 2017 because PM2.5 scavenges hydroperoxy and NO_x radicals that would otherwise produce ozone. In addition to this sensitivity test, we also investigated the trends of NO_x emissions between 1994 and 2016 from the historic Climate Model Intercomparison Project 6 Community Emissions Data System (CMIP6 CEDS), inventory used in the next IPCC report (AR6) and considered to be more up-to-date. We found the same shift of NO_x emissions toward the equator for the same sources (biofuel and fossil fuel). In addition, over 22 years starting in the mid-1990s, the trends of NO_x emissions are still positive above China despite reductions in the most recent years. Given the uncertainties across all emission inventories and the impact of these uncertainties on ozone production (*62*), we do not expect the choice of emission inventory to change the overall conclusion that net ozone production increased across China over the 22-year study period.

In the 11 study regions, the changes of modeled NO_x concentrations in the boundary layer (fig. S4D) have responded to the changes in emissions (fig. S9), as expected. However, the changes in NO_x concentrations in the UT (400 to 200 hPa) do not match the changes at the surface immediately below (fig. S6D). In particular, NO_x concentrations increased in the UT above midlatitudes despite emission reductions at the surface of North America and Europe. The explanation for this increase is linked to the increase of NO_x emissions across southern, southeastern, and eastern Asia (Fig. 5 and figs. S4 and S9), coupled with the well-established transport pathways from the polluted boundary layer of Asia to the UT of northern midlatitudes (*63*–*66*), as simulated by the MERRA-2 GMI model.

In the MERRA-2 GMI model, the stratospheric ozone tracer (fig. S6) shows notable increases above 350 hPa for eastern North America, western North America, and Northeast China/Korea but not above the other regions. These increases are strongest during the cold season (October to March), when the trends can reach 7 nmol mol^{-1} decade^{-1}. The dynamical processes that control stratosphere-to-troposphere transport are known to be highly variable in space and time (*67*), and the increase of the stratospheric ozone tracer above some regions but not others could be related to interannual variability of these transport processes. Within the output of the MERRA-2 GMI model, the stratospheric influence appears to explain much of the modeled ozone increase in the UT above the three midlatitude regions. However, this is probably an overestimate, as the model stratospheric ozone tracer is reported on a particular pressure surface (e.g., 250 hPa) for all air masses, no matter if an air mass is located in the UT or the lowermost stratosphere. In contrast, the observed ozone trend reported for a particular pressure surface (e.g., 250 hPa) is based purely on ozone observations made within the troposphere (all stratospheric air samples were removed, as described in the "IAGOS data" section). Therefore, we expect the actual stratospheric influence on the observed midlatitude ozone trends to be less than that indicated by the model. The stratospheric influence on trends in the subtropical and tropical regions is negligible, as expected, because of the fact that stratosphere-to-troposphere transport occurs predominantly at high latitudes and midlatitudes (*68*).

While the model indicates that stratospheric influence plays a role in the observed ozone increases in the UT above some midlatitude regions, the MT (550 to 350 hPa) ozone increases are largely explained by the transport of ozone and its precursors from low latitudes to midlatitudes, in agreement with the previous model analysis by Zhang *et al.* (*57*).

Impacts on RF

A final analysis focuses on the qualitative relationship between the observed ozone increases and the RF due to tropospheric ozone.

Downloaded from http://advances.sciencemag.org/ on November 10, 2020

The consensus estimate of ozone's global mean RF, for the period 1750–2010, is 0.4 ± 0.2 W m^{-2}, based on an ensemble of models (*2*). A recent analysis by Myhre *et al.* (*8*), based on five global chemistry climate models, determined that the global mean RF due to ozone for the period 1990–2015 is +0.06 ± 0.03 W m^{-2}, a rate of increase that is approximately double the IPCC estimate for the period 1990–2010 [see Fig. 7, Myhre *et al.* (*8*)]. Myhre *et al.* (*8*) also concluded that the strongest increases in tropospheric ozone occurred above the regions of Asia and the Middle East located south of 30°N. An independent analysis reached similar conclusions and also provided analysis to show that the RF is roughly 50% greater in the Northern Hemisphere compared to the global mean (*69*). The study regions in the present analysis are limited to 11 locations in the Northern Hemisphere, and therefore, they cannot provide a global mean value of RF due to ozone, which considers both hemispheres. However, the observations can be used to demonstrate that the models used by Myhre *et al.* (*8*) are generally correct in their determination that recent increases of RF due to ozone are strongest in the tropics. Figure 6 compares RF due to ozone above the 11 study regions to the estimates of IPCC (1990–2010) and Myhre *et al.* (1990–2015). RF values above the 11 study regions were estimated using the same normalized total (shortwave + longwave) RF values adopted by IPCC for estimating future RF from model output (*2*, *70*); this method focuses on TCO and does not account for ozone's vertical distribution. The model estimates are mean values for the entire globe, and therefore, they are heavily weighted by regions of low ozone growth, such as the midlatitudes and high latitudes of the Southern Hemisphere. RF values above the 11 study regions can be much greater than the model estimates because of strong regional increases of ozone that are not representative of the entire globe. In general, the observation-based estimates of RF increase from north to south, with the greatest values above the Middle East, southern regions of Asia, and Malaysia/Indonesia, consistent with the model estimates of Myhre *et al.* (*8*) that show the greatest ozone increases in these same regions. While our results cannot provide a global mean RF due to ozone, these regional increases in RF are supportive of model estimates of increasing RF due to ozone for the recent period of 1990–2015 (*8*). These IAGOS data are now available for evaluating and constraining new model estimates of regional- and global-scale RF due to ozone.

SUPPLEMENTARY MATERIALS

Supplementary material for this article is available at http://advances.sciencemag.org/cgi/content/full/6/34/eaba8272/DC1

REFERENCES AND NOTES

1. P. S. Monks, A. T. Archibald, A. Colette, O. Cooper, M. Coyle, R. Derwent, D. Fowler, C. Granier, K. S. Law, G. E. Mills, D. S. Stevenson, O. Tarasova, V. Thouret, E. von Schneidemesser, R. Sommariva, O. Wild, M. L. Williams, Tropospheric ozone and its precursors from the urban to the global scale from air quality to short-lived climate forcer. *Atmos. Chem. Phys.* **15**, 8889–8973 (2015).
2. IPCC, Climate change 2013: The physical science basis, in *Contribution of Working Group I to the Fifth Assessment Report of the Intergovernmental Panel on Climate Change*, T. F. Stocker, D. Qin, Plattner, G.-K. Plattner, M. Tignor, S. K. Allen, J. Boschung, A. Nauels, Y. Xia, V. Bex, P. M. Midgley, Eds. (Cambridge Univ. Press, 2013), p. 1535.
3. L. Y. Yeung, L. T. Murray, P. Martinerie, E. Witrant, H. T. Hu, A. Banerjee, A. Orsi, J. Chappellaz, Isotopic constraint on the twentieth-century increase in tropospheric ozone. *Nature* **570**, 224–227 (2019).
4. D. Tarasick, I. E. Galbally, O. R. Cooper, M. G. Schultz, G. Ancellet, T. Leblanc, T. J. Wallington, J. Ziemke, X. Liu, M. Steinbacher, J. Staehelin, C. Vigouroux, J. W. Hannigan, O. García, G. Foret, P. Zanis, E. Weatherhead, I. Petropavlovskikh, H. Worden, M. Osman, J. Liu, K.-L. Chang, A. Gaudel, M. Y. Lin, M. Granados-Muñoz, A. M. Thompson, S. J. Oltmans, J. Cuesta, G. Dufour, V. Thouret, B. Hassler, T. Trickl, J. L. Neu, Tropospheric ozone assessment report: Tropospheric ozone from 1877 to 2016, observed levels, trends and uncertainties. *Elem. Sci. Anth.* **7**, 39 (2019).
5. A. Gaudel, O. R. Cooper, G. Ancellet, B. Barret, A. Boynard, J. P. Burrows, C. Clerbaux, P.-F. Coheur, J. Cuesta, E. Cuevas, S. Doniki, G. Dufour, F. Ebojie, G. Foret, O. Garcia, M. J. Granados-Muñoz, J. W. Hannigan, F. Hase, B. Hassler, G. Huang, D. Hurtmans, D. Jaffe, N. Jones, P. Kalabokas, B. Kerridge, S. Kulawik, B. Latter, T. Leblanc, E. Le Flochmoën, W. Lin, J. Liu, X. Liu, E. Mahieu, A. McClure-Begley, J. L. Neu, M. Osman, M. Palm, H. Petetin, I. Petropavlovskikh, R. Querel, N. Rahpoe, A. Rozanov, M. G. Schultz, J. Schwab, R. Siddans, D. Smale, M. Steinbacher, H. Tanimoto, D. W. Tarasick, V. Thouret, A. M. Thompson, T. Trickl, E. Weatherhead, C. Wespes, H. M. Worden, C. Vigouroux, X. Xu, G. Zeng, J. Ziemke, Tropospheric ozone assessment report: Present-day distribution and trends of tropospheric ozone relevant to climate and global atmospheric chemistry model evaluation. *Elem. Sci. Anth.* **6**, 39 (2018).
6. A. Petzold, V. Thouret, C. Gerbig, A. Zahn, C. A. M. Brenninkmeijer, M. Gallagher, M. Hermann, M. Pontaud, H. Ziereis, D. Boulanger, J. Marshall, P. Nédélec, H. G. J. Smit, U. Friess, J.-M. Flaud, A. Wahner, J.-P. Cammas, A. Volz-Thomas; IAGOS Team, Global-scale atmosphere monitoring by in-service aircraft—Current achievements and future prospects of the European Research Infrastructure IAGOS. *Tellus B* **67**, 28452 (2015).
7. Y. Cohen, H. Petetin, V. Thouret, V. Marécal, B. Josse, H. Clark, B. Sauvage, A. Fontaine, G. Athier, R. Blot, D. Boulanger, J.-M. Cousin, P. Nédélec, Climatology and long-term evolution of ozone and carbon monoxide in the upper troposphere–lower stratosphere (UTLS) at northern midlatitudes, as seen by IAGOS from 1995 to 2013. *Atmos. Chem. Phys.* **18**, 5415–5453 (2018).
8. G. Myhre, W. Aas, R. Cherian, W. Collins, G. Faluvegi, M. Flanner, P. Forster, Ø. Hodnebrog, Z. Klimont, M. T. Lund, J. Mülmenstädt, C. L. Myhre, D. Olivié, M. Prather, J. Quaas, B. H. Samset, J. L. Schnell, M. Schulz, D. Shindell, R. B. Skeie, T. Takemura, S. Tsyro, Multi-model simulations of aerosol and ozone radiative forcing due to anthropogenic emission changes during the period 1990–2015. *Atmos. Chem. Phys.* **17**, 2709–2720 (2017).
9. V. Thouret, A. Marenco, J. A. Logan, P. Nédélec, C. Grouhel, Comparisons of ozone measurements from the MOZAIC airborne program and the ozone sounding network at eight locations. *J. Geophys. Res. Atmos.* **103**, 25695–25720 (1998).
10. P. Nédélec, R. Blot, D. Boulanger, G. Athier, J.-M. Cousin, B. Gautron, A. Petzold, A. Volz-Thomas, V. Thouret, Instrumentation on commercial aircraft for monitoring the atmospheric composition on a global scale: The IAGOS system, technical overview of ozone and carbon monoxide measurements. *Tellus B* **67**, 27791 (2015).
11. H. Petetin, V. Thouret, G. Athier, R. Blot, D. Boulanger, J.-M. Cousin, A. Gaudel, P. Nédélec, O. Cooper, Diurnal cycle of ozone throughout the troposphere over Frankfurt as measured by MOZAIC-IAGOS commercial aircraft. *Elem. Sci. Anth.* **4**, 129 (2016).
12. L. D. Oman, A. R. Douglass, J. R. Ziemke, J. M. Rodriguez, D. W. Waugh, J. E. Nielsen, The ozone response to ENSO in Aura satellite measurements and a chemistry-climate simulation. *J. Geophys. Res. Atmos.* **118**, 965–976 (2013).
13. E. A. Barnes, A. M. Fiore, L. W. Horowitz, Detection of trends in surface ozone in the presence of climate variability. *J. Geophys. Res. Atmos.* **121**, 6112–6129 (2016).
14. J. A. Logan, J. Staehelin, I. A. Megretskaia, J.-P. Cammas, V. Thouret, H. Claude, H. De Backer, M. Steinbacher, H.-E. Scheel, R. Stübi, M. Fröhlich, R. Derwent, Changes in ozone over Europe: Analysis of ozone measurements from sondes, regular aircraft (MOZAIC) and alpine surface sites. *J. Geophys. Res. Atmos.* **117**, D09301 (2012).
15. H. Petetin, M. Jeoffrion, B. Sauvage, G. Athier, R. Blot, D. Boulanger, H. Clark, J.-M. Cousin, F. Gheusi, P. Nédélec, M. Steinbacher, V. Thouret, Representativeness of the IAGOS airborne measurements in the lower troposphere. *Elem. Sci. Anth.* **6**, 23 (2018).
16. J. Staufer, J. Staehelin, R. Stübi, T. Peter, F. Tummon, V. Thouret, Trajectory matching of ozonesondes and MOZAIC measurements in the UTLS—Part 1: Method description and application at Payerne, Switzerland. *Atmos. Meas. Tech.* **6**, 3393–3406 (2013).
17. J. Staufer, J. Staehelin, R. Stübi, T. Peter, F. Tummon, V. Thouret, Trajectory matching of ozonesondes and MOZAIC measurements in the UTLS—Part 2: Application to the global ozonesonde network. *Atmos. Meas. Tech.* **7**, 241–266 (2014).
18. A. Molod, L. Takacs, M. Suarez, J. Bacmeister, Development of the GEOS-5 atmospheric general circulation model: Evolution from MERRA to MERRA2. *Geosci. Model Dev.* **8**, 1339–1356 (2015).
19. C. Orbe, L. D. Oman, S. E. Strahan, D. W. Waugh, S. Pawson, L. L. Takacs, A. M. Molod, Large-scale atmospheric transport in GEOS replay simulations. *J. Adv. Model Earth Syst.* **9**, 2545–2560 (2017).
20. R. Gelaro, W. McCarty, M. J. Suárez, R. Todling, A. Molod, L. Takacs, C. A. Randles, A. Darmenov, M. G. Bosilovich, R. Reichle, K. Wargan, L. Coy, R. Cullather, C. Draper, S. Akella, V. Buchard, A. Conaty, A. M. da Silva, W. Gu, G.-K. Kim, R. Koster, R. Lucchesi, D. Merkova, J. E. Nielsen, G. Partyka, S. Pawson, W. Putman, M. Rienecker, S. D. Schubert, M. Sienkiewicz, B. Zhao, The modern-era retrospective analysis for research and applications, version 2 (MERRA-2). *J. Climate* **30**, 5419–5454 (2017).
21. B. N. Duncan, S. E. Strahan, Y. Yoshida, S. D. Steenrod, N. Livesey, Model study of the cross-tropopause transport of biomass burning pollution. *Atmos. Chem. Phys.* **7**, 3713–3736 (2007).

Downloaded from http://advances.sciencemag.org/ on November 10, 2020

22. J. E. Nielsen, S. Pawson, A. Molod, B. Auer, A. M. da Silva, A. R. Douglass, B. Duncan, Q. Liang, M. Manyin, L. D. Oman, W. Putman, S. E. Strahan, K. Wargan, Chemical mechanisms and their applications in the Goddard Earth Observing System (GEOS) earth system model. *J. Adv. Model Earth Syst.* **9**, 3019–3044 (2017).
23. J. R. Ziemke, L. D. Oman, S. A. Strode, A. R. Douglass, M. A. Olsen, R. D. McPeters, P. K. Bhartia, L. Froidevaux, G. J. Labow, J. C. Witte, A. M. Thompson, D. P. Haffner, N. A. Kramarova, S. M. Frith, L.-K. Huang, G. R. Jaross, C. J. Seftor, M. T. Deland, S. L. Taylor, Trends in global tropospheric ozone inferred from a composite record of TOMS/OMI/MLS/OMPS satellite measurements and the MERRA-2 GMI simulation. *Atmos. Chem. Phys.* **19**, 3257–3269 (2019).
24. C. Granier, B. Bessagnet, T. Bond, A. D'Angiola, H. D. van der Gon, G. J. Frost, A. Heil, J. W. Kaiser, S. Kinne, Z. Klimont, S. Kloster, J.-F. Lamarque, C. Liousse, T. Masui, F. Meleux, A. Mieville, T. Ohara, J.-C. Raut, K. Riahi, M. G. Schultz, S. J. Smith, A. Thompson, J. van Aardenne, G. R. van der Werf, D. P. van Vuuren, Evolution of anthropogenic and biomass burning emissions of air pollutants at global and regional scales during the 1980–2010 period. *Clim. Change* **109**, 163–190 (2011).
25. N. A. Krotkov, C. A. McLinden, C. Li, L. N. Lamsal, E. A. Celarier, S. V. Marchenko, W. H. Swartz, E. J. Bucsela, J. Joiner, B. N. Duncan, K. F. Boersma, J. P. Veefkind, P. F. Levelt, V. E. Fioletov, R. R. Dickerson, H. He, Z. F. Lu, D. G. Streets, Aura OMI observations of regional SO_2 and NO_2 pollution changes from 2005 to 2015. *Atmos. Chem. Phys.* **16**, 4605–4629 (2016).
26. F. Liu, S. Beirle, Q. Zhang, R. J. van der A, B. Zheng, D. Tong, K. B. He, NO_x emission trends over Chinese cities estimated from OMI observations during 2005 to 2015. *Atmos. Chem. Phys.* **17**, 9261–9275 (2017).
27. G. R. van der Werf, J. T. Randerson, L. Giglio, T. T. van Leeuwen, Y. Chen, B. M. Rogers, M. Q. Mu, M. J. E. van Marle, D. C. Morton, G. J. Collatz, R. J. Yokelson, P. S. Kasibhatla, Global fire emissions estimates during 1997–2016. *Earth Syst. Sci. Data* **9**, 697–720 (2017).
28. D. Allen, K. Pickering, B. Duncan, M. Damon, Impact of lightning NO emissions on North American photochemistry as determined using the Global Modeling Initiative (GMI) model. *J. Geophys. Res. Atmos.* **115**, D22301 (2010).
29. C. H. Song, G. Chen, S. R. Hanna, J. Crawford, D. D. Davis, Dispersion and chemical evolution of ship plumes in the marine boundary layer: Investigation of $O_3/NO_y/HO_x$ chemistry. *J. Geophys. Res. Atmos.* **108**, 4143 (2003).
30. Q. Liang, A. R. Douglass, B. N. Duncan, R. S. Stolarski, J. C. Witte, The governing processes and timescales of stratosphere-to-troposphere transport and its contribution to ozone in the Arctic troposphere. *Atmos. Chem. Phys.* **9**, 3011–3025 (2009).
31. R. Koenker, G. Bassett Jr., Regression quantiles. *Econometrica* **46**, 33–50 (1978).
32. R. Koenker, Z. J. Xiao, Inference on the quantile regression process. *Econometrica* **70**, 1583–1612 (2002).
33. B. S. Cade, B. R. Noon, A gentle introduction to quantile regression for ecologists. *Front. Ecol. Environ.* **1**, 412–420 (2003).
34. C. Davino, M. Furno, D. Vistocco, in *Quantile Regression: Theory and Applications* (Wiley Series in Probability and Statistics, Wiley, 2014), pp. 1–260.
35. R. L. Wasserstein, N. A. Lazar, The ASA's statement on *P* values: Context, process, and purpose. *Am. Stat.* **70**, 129–131 (2016).
36. R. L. Wasserstein, A. L. Schirm, N. A. Lazar, Moving to a world beyond "$p < 0.05$". *Am. Stat.* **73**, 1–19 (2019).
37. V. Amrhein, S. Greenland, B. McShane, Scientists rise up against statistical significance. *Nature* **567**, 305–307 (2019).
38. European Environmental Agnecy, Air Quality in Europe—2016 Report, EEA Report No 28/2016 (2016); http://eea.europa.eu/publications/air-quality-in-europe-2016.
39. H. Simon, A. Reff, B. Wells, J. Xing, N. Frank, Ozone trends across the United States over a period of decreasing NOx and VOC emissions. *Environ. Sci. Technol.* **49**, 186–195 (2015).
40. K. L. Chang, I. Petropavlovskikh, O. R. Cooper, M. G. Schultz, T. Wang, Regional trend analysis of surface ozone observations from monitoring networks in eastern North America, Europe and East Asia. *Elem. Sci. Anth.* **5**, 50 (2017).
41. J. E. Johnson, R. H. Gammon, J. Larsen, T. S. Bates, S. J. Oltmans, J. C. Farmer, Ozone in the marine boundary layer over the Pacific and Indian oceans: Latitudinal gradients and diurnal cycles. *J. Geophys. Res. Atmos.* **95**, 11847–11856 (1990).
42. S. J. Oltmans, B. J. Johnson, J. M. Harris, A. M. Thompson, H. Y. Liu, C. Y. Chan, H. Vömel, T. Fujimoto, V. G. Brackett, W. L. Chang, J. P. Chen, J. H. Kim, L. Y. Chan, H.-W. Chang, Tropospheric ozone over the North Pacific from ozonesonde observations. *J. Geophys. Res. Atmos.* **109**, D15S01 (2004).
43. S. J. Oltmans, B. J. Johnson, J. M. Harris, H. Vömel, A. M. Thompson, K. Koshy, P. Simon, R. J. Bendura, J. A. Logan, F. Hasebe, M. Shiotani, V. W. J. H. Kirchhoff, M. Maata, G. Sami, A. Samad, J. Tabuadravu, H. Enriquez, M. Agama, J. Cornejo, F. Paredes, Ozone in the Pacific tropical troposphere from ozonesonde observations. *J. Geophys. Res. Atmos.* **106**, 32503–32525 (2001).
44. E. V. Browell, M. A. Fenn, C. F. Butler, W. B. Grant, S. Ismail, R. A. Ferrare, S. A. Kooi, V. G. Brackett, M. B. Clayton, M. A. Avery, J. D. W. Barrick, H. E. Fuelberg, J. C. Maloney, R. E. Newell, Y. Zhu, M. J. Mahoney, B. E. Anderson, D. R. Blake, W. H. Brune, B. G. Heikes, G. W. Sachse, H. B. Singh, R. W. Talbot, Large-scale air mass characteristics observed over the remote tropical Pacific Ocean during March–April 1999: Results from PEM-Tropics B field experiment. *J. Geophys. Res. Atmos.* **106**, 32481–32501 (2001).
45. D. Kley, P. J. Crutzen, H. G. J. Smit, H. Vomel, S. J. Oltmans, H. Grassl, V. Ramanathan, Observations of near-zero ozone concentrations over the convective Pacific: Effects on air chemistry. *Science* **274**, 230–233 (1996).
46. M. G. Lawrence, P. J. Crutzen, P. J. Rasch, Analysis of the CEPEX ozone data using a 3D chemistry–meteorology model. *Q. J. R. Meteorol. Soc.* **125**, 2987–3009 (1999).
47. R. Newton, G. Vaughan, E. Hintsa, M. T. Filus, L. L. Pan, S. Honomichl, E. Atlas, S. J. Andrews, L. J. Carpenter, Observations of ozone-poor air in the tropical tropopause layer. *Atmos. Chem. Phys.* **18**, 5157–5171 (2018).
48. W. A. H. Asman, M. G. Lawrence, C. A. M. Brenninkmeijer, P. J. Crutzen, J. W. M. Cuijpers, P. Nédélec, Rarity of upper-tropospheric low O_3 mixing ratio events during MOZAIC flights. *Atmos. Chem. Phys.* **3**, 1541–1549 (2003).
49. W. B. Grant, E. V. Browell, C. F. Butler, M. A. Fenn, M. B. Clayton, J. R. Hannan, H. E. Fuelberg, D. R. Blake, N. J. Blake, G. L. Gregory, B. G. Heikes, G. W. Sachse, H. B. Singh, J. Snow, R. W. Talbot, A case study of transport of tropical marine boundary layer and lower tropospheric air masses to the northern midlatitude upper troposphere. *J. Geophys. Res. Atmos.* **105**, 3757–3769 (2000).
50. W. E. Davies, G. Vaughan, F. M. O'Connor, Observation of near-zero ozone concentrations in the upper troposphere at mid-latitudes. *Geophys. Res. Lett.* **25**, 1173–1176 (1998).
51. J. L. Moody, S. J. Oltmans, H. Levy II, J. T. Merrill, Transport, climatology of tropospheric ozone: Bermuda, 1988–1991. *J. Geophys. Res. Atmos.* **100**, 7179–7194 (1995).
52. O. R. Cooper, J. L. Moody, J. C. Davenport, S. J. Oltmans, B. J. Johnson, X. Chen, P. B. Shepson, J. T. Merrill, Influence of springtime weather systems on vertical ozone distributions over three North American sites. *J. Geophys. Res. Atmos.* **103**, 22001–22013 (1998).
53. O. R. Cooper, D. D. Parrish, A. Stohl, M. Trainer, P. Nédélec, V. Thouret, J. P. Cammas, S. J. Oltmans, B. J. Johnson, D. Tarasick, T. Leblanc, I. S. McDermid, D. Jaffe, R. Gao, J. Stith, T. Ryerson, K. Aikin, T. Campos, A. Weinheimer, M. A. Avery, Increasing springtime ozone mixing ratios in the free troposphere over western North America. *Nature* **463**, 344–348 (2010).
54. S. Yonemura, H. Tsuruta, S. Kawashima, S. Sudo, L. C. Peng, L. S. Fook, Z. Johar, M. Hayashi, Tropospheric ozone climatology over Peninsular Malaysia from 1992 to 1999. *J. Geophys. Res. Atmos.* **107**, D15 (2002).
55. A. M. Thompson, S. K. Miller, S. Tilmes, D. W. Kollonige, J. C. Witte, S. J. Oltmans, B. J. Johnson, M. Fujiwara, F. J. Schmidlin, G. J. R. Coetzee, N. Komala, M. Maata, M. Mohamad, J. Nguyo, C. Mutai, S.-Y. Ogino, F. R. Da Silva, N. M. P. Leme, F. Posny, R. Scheele, H. B. Selkirk, M. Shiotani, R. Stübi, G. Levrat, B. Calpini, V. Thouret, H. Tsuruta, J. V. Canossa, H. Vömel, S. Yonemura, J. A. Diaz, N. T. Tan Thanh, H. T. Thuy Ha, Southern Hemisphere Additional Ozonesondes (SHADOZ) ozone climatology (2005–2009): Tropospheric and tropical tropopause layer (TTL) profiles with comparisons to OMI-based ozone products. *J. Geophys. Res. Atmos.* **117**, D23301 (2012).
56. M. J. Cooper, R. V. Martin, N. J. Livesey, D. A. Degenstein, K. A. Walker, Analysis of satellite remote sensing observations of low ozone events in the tropical upper troposphere and links with convection. *Geophys. Res. Lett.* **40**, 3761–3765 (2013).
57. Y. Zhang, O. R. Cooper, A. Gaudel, A. M. Thompson, P. Nédélec, S.-Y. Ogino, J. J. West, Tropospheric ozone change from 1980 to 2010 dominated by equatorward redistribution of emissions. *Nat. Geosci.* **9**, 875–879 (2016).
58. L. T. Murray, Erratum to: Lightning NO_x and impacts on air quality. *Curr. Pollut. Rep.* **2**, 134–134 (2016).
59. R. J. van der A, B. Mijling, J. Ding, M. E. Koukouli, F. Liu, Q. Li, H. Q. Mao, N. Theys, Cleaning up the air: Effectiveness of air quality policy for SO_2 and NO_x emissions in China. *Atmos. Chem. Phys.* **17**, 1775–1789 (2017).
60. X. Lu, J. Y. Hong, L. Zhang, O. R. Cooper, M. G. Schultz, X. B. Xu, T. Wang, M. Gao, Y. H. Zhao, Y. H. Zhang, Severe surface ozone pollution in China: A global perspective. *Environ. Sci. Tech. Lett.* **5**, 487–494 (2018).
61. K. Li, D. J. Jacob, H. Liao, J. Zhu, V. Shah, L. Shen, K. H. Bates, Q. Zhang, S. Zhai, A two-pollutant strategy for improving ozone and particulate air quality in China. *Nat. Geosci.* **12**, 906–910 (2019).
62. I. Bouarar, G. Brasseur, K. Petersen, C. Granier, Q. Fan, X. M. Wang, L. L. Wang, D. S. Ji, Z. R. Liu, Y. Xie, W. Gao, N. Elguindi, Influence of anthropogenic emission inventories on simulations of air quality in China during winter and summer 2010. *Atmos. Environ.* **198**, 236–256 (2019).
63. J. A. de Gouw, O. R. Cooper, C. Warneke, P. K. Hudson, F. C. Fehsenfeld, J. S. Holloway, G. Hübler, D. K. Nicks Jr., J. B. Nowak, D. D. Parrish, T. B. Ryerson, E. L. Atlas, S. G. Donnelly, S. M. Schauffler, V. Stroud, K. Johnson, G. R. Carmichael, D. G. Streets, Chemical composition of air masses transported from Asia to the U.S. West Coast during ITCT 2K2: Fossil fuel combustion versus biomass-burning signatures. *J. Geophys. Res. Atmos.* **109**, D23S20 (2004).
64. C. Forster, O. Cooper, A. Stohl, S. Eckhardt, P. James, E. Dunlea, D. K. Nicks Jr., J. S. Holloway, G. Hübler, D. D. Parrish, T. B. Ryerson, M. Trainer, Lagrangian transport model forecasts and a transport climatology for the Intercontinental Transport

Downloaded from http://advances.sciencemag.org/ on November 10, 2020

and Chemical Transformation 2002 (ITCT 2K2) measurement campaign. *J. Geophys. Res. Atmos.* **109**, D07S92 (2004).
65. O. R. Cooper, A. Stohl, S. Eckhardt, D. D. Parrish, S. J. Oltmans, B. J. Johnson, P. Nédélec, F. J. Schmidlin, M. J. Newchurch, Y. Kondo, K. Kita, A springtime comparison of tropospheric ozone and transport pathways on the east and west coasts of the United States. *J. Geophys. Res. Atmos.* **110**, D05S90 (2005).
66. O. R. Cooper, S. J. Oltmans, B. J. Johnson, J. Brioude, W. Angevine, M. Trainer, D. D. Parrish, T. R. Ryerson, I. Pollack, P. D. Cullis, M. A. Ives, D. W. Tarasick, J. Al-Saadi, I. Stajner, Measurement of western U.S. baseline ozone from the surface to the tropopause and assessment of downwind impact regions. *J. Geophys. Res. Atmos.* **116**, D00V03 (2011).
67. J. L. Neu, T. Flury, G. L. Manney, M. L. Santee, N. J. Livesey, J. Worden, Tropospheric ozone variations governed by changes in stratospheric circulation. *Nat. Geosci.* **7**, 340–344 (2014).
68. B. Škerlak, M. Sprenger, H. Wernli, A global climatology of stratosphere–troposphere exchange using the ERA-Interim data set from 1979 to 2011. *Atmos. Chem. Phys.* **14**, 913–937 (2014).
69. R. Checa-Garcia, M. I. Hegglin, D. Kinnison, D. A. Plummer, K. P. Shine, Historical tropospheric and stratospheric ozone radiative forcing using the CMIP6 database. *Geophys. Res. Lett.* **45**, 3264–3273 (2018).
70. D. S. Stevenson, P. J. Young, V. Naik, J.-F. Lamarque, D. T. Shindell, A. Voulgarakis, R. B. Skeie, S. B. Dalsoren, G. Myhre, T. K. Berntsen, G. A. Folberth, S. T. Rumbold, W. J. Collins, I. A. MacKenzie, R. M. Doherty, G. Zeng, T. P. C. van Noije, A. Strunk, D. Bergmann, P. Cameron-Smith, D. A. Plummer, S. A. Strode, L. Horowitz, Y. H. Lee, S. Szopa, K. Sudo, T. Nagashima, B. Josse, I. Cionni, M. Righi, V. Eyring, A. Conley, K. W. Bowman, O. Wild, A. Archibald, Tropospheric ozone changes, radiative forcing and attribution to emissions in the Atmospheric Chemistry and Climate Model Intercomparison Project (ACCMIP). *Atmos. Chem. Phys.* **13**, 3063–3085 (2013).

Acknowledgment: We acknowledge the support of the European Commission, Airbus, and the Airlines (Lufthansa, Air France, Austrian, Air Namibia, Cathay Pacific, Iberia, China Airlines, and Hawaiian Airlines) that carry the MOZAIC or IAGOS equipment and perform the maintenance since 1994. **Funding:** A.G., O.R.C., K.-L.C., and I.B. were supported by the Cooperative Institute for Research in Environmental Sciences, University of Colorado, Boulder. V.T., P.N., and R.B. were supported by IAGOS which receives funding from the European Commission, National Research Programmes in Germany (BMBF), France (INSU-CNRS, MESR, and CNES), and United Kingdom (NERC). The MERRA-2 GMI simulation was funded by the NASA MAP program. S.A.S. was supported by the NASA MAP and ACMAP programs. In its last 10 years of operation, MOZAIC was funded by INSU-CNRS (France), Météo-France, Université Paul Sabatier (Toulouse, France), and Research Center Jülich (FZJ, Jülich, Germany). IAGOS has been additionally funded by the EU projects IAGOS-DS and IAGOS-ERI. The MOZAIC-IAGOS database was supported by AERIS (CNES and INSU-CNRS). **Author contributions:** Conceptualization: A.G. and O.R.C. Formal analysis: A.G., K.-L.C., I.B., S.A.S., J.R.Z., and P.S. Investigation: A.G. Methodology: A.G., K.-L.C., O.R.C, and C.G. Resources: V.T., R.B., P.N., S.A.S., and L.D.O. Supervision: O.R.C. and A.G. Visualization: A.G., O.R.C., I.B., and S.A.S. Writing (original draft): A.G. Writing (review and editing): A.G., O.R.C., K.-L.C., I.B., S.A.S., J.R.Z., P.S., V.T., R.B., P.N., L.D.O., and C.G. **Competing interests:** The authors declare that they have no competing interests. **Data and materials availability:** Aircraft campaigns: Data from ATom, HIPPO, Arctas, TOTE VOTE, AASE2 and AASE can be found at https://daac.ornl.gov/ATOM/campaign/, www.eol.ucar.edu/field_projects/hippo, www-air.larc.nasa.gov/missions/arctas/dataaccess.htm, https://espo.nasa.gov/crystalface/archive/browse/tote, https://espo.nasa.gov/aase/archive/browse/aase2/DC8, and https://espo.nasa.gov/aase/archive/browse/aase/DC8, respectively. Ozonesonde above Hilo, Hawaii: Ozonesonde data above Hilo, Hawaii are publicly available at ftp://aftp.cmdl.noaa.gov/data/ozwv/Ozonesonde/. IAGOS data: IAGOS data are publicly available at https://doi.org/10.25326/20. Surface emissions: MACCity emissions are publicly available at eccad.aeris-data.fr/. OMI/MLS TCO data are available at https://acd-ext.gsfc.nasa.gov/Data_services/cloud_slice/.

Submitted 8 January 2020
Accepted 9 July 2020
Published 21 August 2020
10.1126/sciadv.aba8272

Citation: A. Gaudel, O. R. Cooper, K.-L. Chang, I. Bourgeois, J. R. Ziemke, S. A. Strode, L. D. Oman, P. Sellitto, P. Nédélec, R. Blot, V. Thouret, C. Granier, Aircraft observations since the 1990s reveal increases of tropospheric ozone at multiple locations across the Northern Hemisphere. *Sci. Adv.* **6**, eaba8272 (2020).

Downloaded from http://advances.sciencemag.org/ on November 10, 2020

Science Advances

Aircraft observations since the 1990s reveal increases of tropospheric ozone at multiple locations across the Northern Hemisphere

Audrey Gaudel, Owen R. Cooper, Kai-Lan Chang, Ilann Bourgeois, Jerry R. Ziemke, Sarah A. Strode, Luke D. Oman, Pasquale Sellitto, Philippe Nédélec, Romain Blot, Valérie Thouret and Claire Granier

Sci Adv **6** (34), eaba8272.
DOI: 10.1126/sciadv.aba8272

ARTICLE TOOLS http://advances.sciencemag.org/content/6/34/eaba8272

SUPPLEMENTARY MATERIALS http://advances.sciencemag.org/content/suppl/2020/08/17/6.34.eaba8272.DC1

REFERENCES This article cites 67 articles, 1 of which you can access for free
http://advances.sciencemag.org/content/6/34/eaba8272#BIBL

PERMISSIONS http://www.sciencemag.org/help/reprints-and-permissions

Use of this article is subject to the Terms of Service

Science Advances (ISSN 2375-2548) is published by the American Association for the Advancement of Science, 1200 New York Avenue NW, Washington, DC 20005. The title *Science Advances* is a registered trademark of AAAS.

Copyright © 2020 The Authors, some rights reserved; exclusive licensee American Association for the Advancement of Science. No claim to original U.S. Government Works. Distributed under a Creative Commons Attribution NonCommercial License 4.0 (CC BY-NC).

Downloaded from http://advances.sciencemag.org/ on November 10, 2020